Supporting Information

Amorphous PtO_x-Engineered $Pt@WO_3$ Nanozymes with Efficient NAD^+ Generation for an Electrochemical Cascade Biosensor

Xinting Liu,[a] Wanyi Zhang,[a] Minghui Yang,[a,c,d]* and Xingxing Jiang[b,c,d]*

[a]Hunan Provincial Key Laboratory of Micro & Nano Materials Interface Science, College of Chemistry and Chemical Engineering, Central South University, Changsha 410083, China.

[b]Department of Dermatology, Xiangya Hospital, Central South University, Changsha 410008, China.

[c]Furong Laboratory, Changsha, 410083, China.

[d]National Engineering Research Center of Personalized Diagnostic and Therapeutic Technology, Changsha, 410083, China.

Corresponding Author:

yangminghui@csu.edu.cn (M. Yang)

xxjjjiang@gmail.com (X. Jiang)

Table of Contents

1. Reagents

NADH (nicotinamide adenine dinucleotide, reduced form), NAD^+ (nicotinamide adenine dinucleotide, oxidized form), benzyl alcohol, tungsten chloride (WCl_6), formaldehyde solution (HCHO), chloroplatinic acid ($H_2PtCl_6 \cdot 6H_2O$), ascorbic Acid (AA), uric acid (UA), and lactic acid (LA) were purchased from Aladdin (Shanghai). Alcohol dehydrogenase (AHD), β-hydroxybutyrate (HB), and β-hydroxybutyrate dehydrogenase (HBD) were purchased from Yuanye (Shanghai). MTS (G3580) was purchased from Promega (Madison, USA). Glucose was purchased from Hengxing Reagent Co., Ltd. Citric Acid was purchased from Huihong Reagent Co., Ltd. $Na_2HPO_4 \cdot 12H_2O$ was purchased from Macklin. Anhydrous ethanol was purchased from Tianjin Zhiyuan Chemical Co., Ltd. Acetone was purchased from Chengdu Cologne Chemical Co., Ltd. The water used to prepare the solutions in the experiment was ultrapure water. The human serum was provided by Xiangya Hospital and was all normal human serum.

2. Characterization

All electrochemical measurements were performed on a CHI-650D electrochemical workstation (Shanghai Chenhua Instrument Co., Ltd., China). In this work, the assay was performed using a conventional three-electrode system consisting of a working electrode (3 mm diameter glassy carbon electrode), an Ag/AgCl reference electrode, and a platinum wire auxiliary electrode. Scanning electron microscopy (SEM) was characterized using JEOL/JSM-7610FPlus (Japan). Transmission electron microscopy (TEM) was characterized using JEOL/JEM-F200 (Japan). X-ray polycrystalline powder diffraction (XRD) was characterized using Ultima IV (Japan). X-ray photoelectron spectra were characterized by AXIS SUPRA+ (Japan). Both superoxide radicals and oxygen vacancies were characterized using an electron paramagnetic resonance spectrometer model Bruker EMXplus-6/1 (Germany). Measurements were performed at 490 nm using an ELx800 enzyme labeler (Bio tek, China). The annealing process uses the OTX-200 (Hefei) tube furnace. UV−vis spectroscopy measurements were performed by using NanoDrop OneC (Thermo American). Raman scattering spectrum was recorded with a Renishaw/inVia Reflex using the 785 nm excitation.

3. Experimental Section

3.1 Preparation of $Pt@WO_3$ and $Pt/PtO_x@WO_{3-x}$.

Following minor modifications to the literature,[1] 100 mg of WCl_6 was dispersed in 30 mL of benzyl alcohol and stirred. When the solution turned light blue, 400 mL of HCHO was added, followed by the dropwise addition of H_2PtCl_6 aqueous solution (4 mL, 10 mmol L^{-1}). After an

additional 10 minutes of stirring, the mixture was transferred to a 100 mL hydrothermal autoclave and reacted at 180 °C for 12 hours. Subsequently, the products were isolated via centrifugation at 12,000 rpm for 10 minutes and washed twice with acetone, ethanol, and deionized water, respectively. After lyophilization, Pt NPs loaded on WO_3 nanosheets ($Pt@WO_3$) were obtained. These nanosheets were then annealed in Ar atmosphere at different temperatures (350 °C, 450 °C, 550 °C, and 650 °C) for 2 hours, yielding 350-$Pt/PtO_x@WO_{3-x}$, 450-$Pt/PtO_x@WO_{3-x}$, 550-$Pt/PtO_x@WO_{3-x}$, and 650-$Pt/PtO_x@WO_{3-x}$ nanosheets.

3.2 The NADH oxidase-like activity of $Pt/PtO_x@WO_{3-x}$.

In standard experiments, the reaction mixture consists of NADH (20 μL, 0.2 mM), $Pt@WO_3$ or $Pt/PtO_x@WO_{3-x}$ (200 μL, 1 mg mL^{-1}), and disodium hydrogen phosphate-citrate buffer (780 μL, 0.2 M, pH=7). After a certain reaction at room temperature, the nanozymes were separated by centrifugation, and the change in NADH absorbance at 340 nm was measured using a UV-vis spectrophotometer. After 60 minutes incubation at room temperature, 20 μL HRP (0.1 mg mL^{-1}) and 100 μL TMB (10 mM) were added into the above solution, and the absorbance at 652 nm was measured using a UV-vis spectrophotometer. Subsequently, the optimal pH, temperature and reaction time of the NADH-catalyzed reaction were investigated.

In the steady-state kinetic assessment, $Pt/PtO_x@WO_{3-x}$ (20 μL, 1 mg mL^{-1}), MTS (3-(4,5-dimethylthiazol-2-yl)-5-(3-carboxy-me-thoxyphenyl)-2-(4-sulfophenyl)-2H-tetrazolium) (20 μL) and NADH (1-10 mM) were sequentially added into a 96-well plate at room temperature under neutral pH, resulting in a color change from yellow to purple. The absorbance at 490 nm was monitored over time using a BioTek microplate reader. The concentration of oxidized NADH was calculated using a molar absorption coefficient of 24000 mol^{-1} L cm^{-1}. The dynamic parameters (K_m and V_{max}) were determined using the Michaelis-Menten equation.

$$V_0 = \frac{V_{max} \times [S]}{K_m + [S]}$$

3.3 The oxidation and recovery of NADH.

To confirm that NADH oxidation yielded biologically active NAD^+, the nanozymes were isolated via centrifugation after a 60-minute reaction of NADH (0.2 mM) with 650-$Pt/PtO_x@WO_{3-x}$ (0.2 mg mL^{-1}). Subsequently, 134 U of ethanol dehydrogenase (ADH) and 5 μL of anhydrous ethanol were introduced, and the absorbance of NADH at 340 nm was continuously monitored at 5-minute intervals.

3.4 Theoretical calculations.

All density functional theory (DFT) calculations were performed by the projector-augmented wave (PAW) method using the Vienna ab initio Simulation Package (version 5.4.4).[2] The Perdew–Burke–Ernzerhof (PBE) form of the generalized gradient approximation (GGA) was adopted to describe the exchange-correlation function.[3] The van der Waals interactions between

substrate and adsorbate were considered by the DFT-D3 method.[4] The kinetic cut-off energy was set to 450 eV and a 2 × 2 × 1 k-points mesh was used for the first Brillouin sampling. All structures were fully relaxed by the conjugate-gradient algorithm until the total energy and Hellmann-Feynman force are less than 1×10^{-5} eV and 0.05 eV $Å^{-1}$, respectively. The Pt supercell was set to 4 × 4 × 3 with a vacuum distance of about 15 Å to ensure negligible interaction.[5] All geometric structures were visualized using the VESTA package.[6]

3.5 Electrochemical performance of the 650-Pt/PtO_x@WO_{3-x}.

The bare glassy carbon electrode (GCE) was polished using 0.05 mm alumina powder and sequentially rinsed with water, ethanol, and deionized water. The 650-Pt/PtO_x@WO_{3-x}/glassy carbon electrode was prepared by a drop-coating method. The working electrodes were either bare GCE or GCE with 650-Pt/PtO_x@WO_{3-x} (5 μL, 2 mg mL^{-1}). The electrochemical properties of 650-Pt/PtO_x@WO_{3-x} were assessed in either blank phosphate-buffered saline (PBS) or PBS containing NADH (2 mM). A platinum wire served as the auxiliary electrode, and an Ag/AgCl electrode functioned as the reference electrode. Cyclic voltammetry (CV) experiments were conducted from -0.4 V to 1.2 V at a scan rate of 50 mV s^{-1}.

3.6 Fabrication of bioelectrodes and detection of HB.

650-Pt/PtO_x@WO_{3-x} (5 μL, 2 mg mL^{-1}) was drop-cast onto the clean GCE surface and dried with an IR lamp. Then, 5 μL of HBD (β-hydroxybutyrate dehydrogenase) /NAD^+ mixture (V_{HBD}/V_{NAD^+}=1:2) was added and dried at room temperature. The electrochemical performance of 650-Pt/PtO_x@WO_{3-x}/HBD-NAD^+/GCE for HB detection were investigated using CV and square wave voltammetry (SWV), with SWV test potentials ranging from 0 to 1.0 V (vs SCE). For the selectivity tests, ascorbic acid (AA, 0.1 mM), glucose (0.8 mM), lactic acid (LA, 1.0 mM), and uric acid (UA, 0.1 mM) were used. Sensor stability test was conducted. The prepared enzyme bioelectrode was stored at 4°C in the refrigerator and tested towards 1 mM HB every day during 7 days.

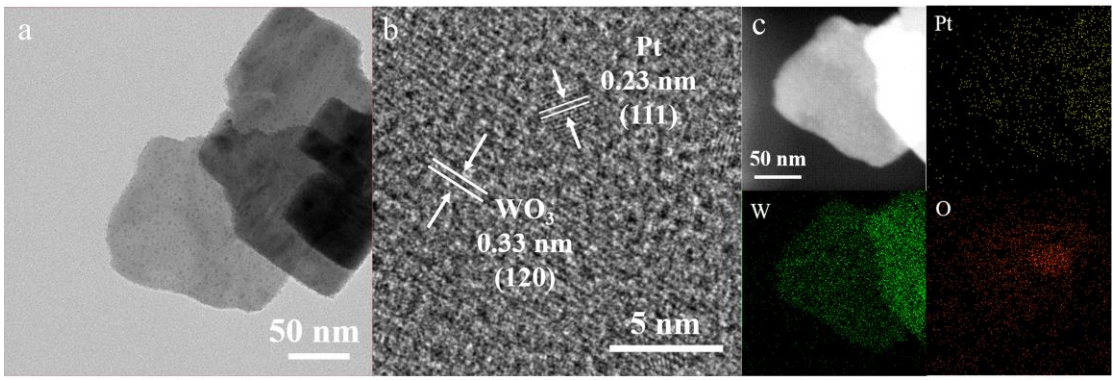

Figure S1. (a) TEM; (b) HRTEM; (c) HAADF-STEM images and corresponding elemental maps of $Pt@WO_3$.

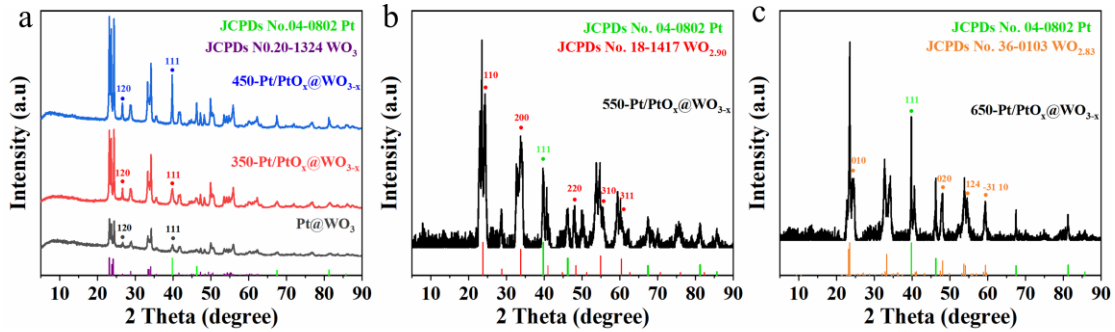

Figure S2. XRD maps of (a) $Pt@WO_3$, 350-$Pt/PtO_x@WO_{3-x}$, and 450-$Pt/PtO_x@WO_{3-x}$; (b) 550-$Pt/PtO_x@WO_{3-x}$; (c) 650-$Pt/PtO_x@WO_{3-x}$.

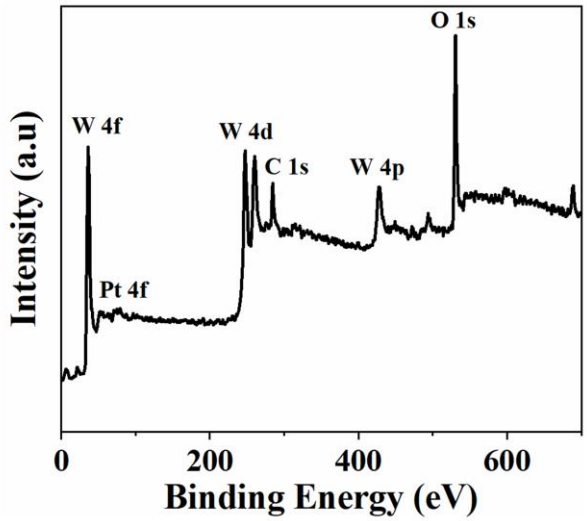

Figure S3. Full XPS spectrum of the as-obtained $Pt@WO_3$ hybrids.

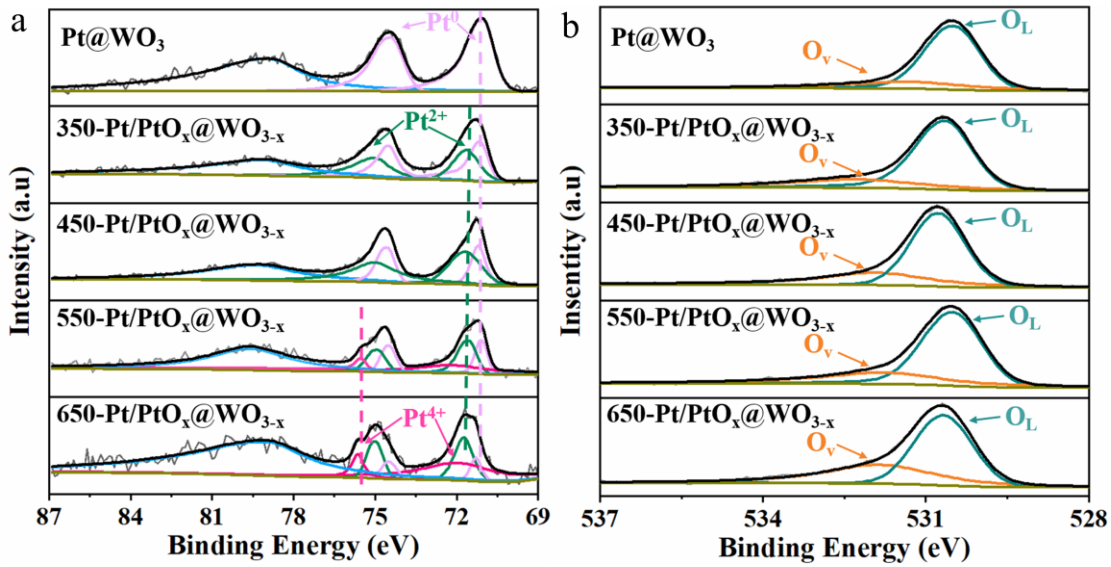

Figure S4. (a) High-resolution XPS orbital profiles of Pt 4f; (b) High-resolution XPS orbital profiles of O 1s.

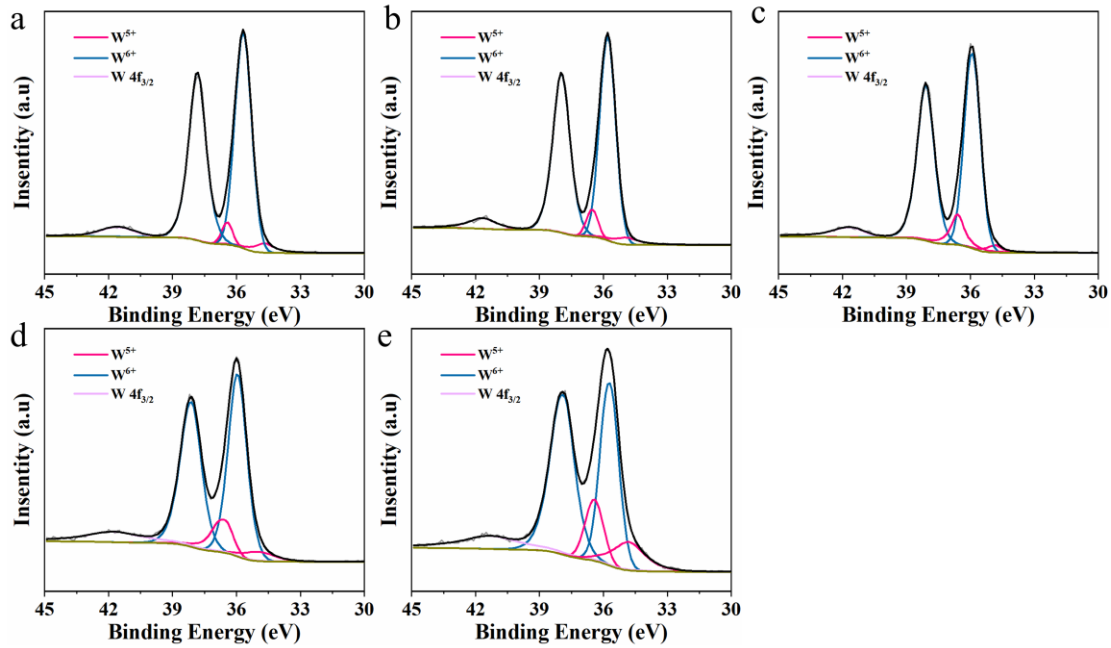

Figure S5. High-resolution XPS W 4f orbital profiles of (a) $Pt@WO_3$; (b) 350-$Pt/PtO_x@WO_{3-x}$; (c) 450-$Pt/PtO_x@WO_{3-x}$; (d) 550-$Pt/PtO_x@WO_{3-x}$; (e) 650-$Pt/PtO_x@WO_{3-x}$.

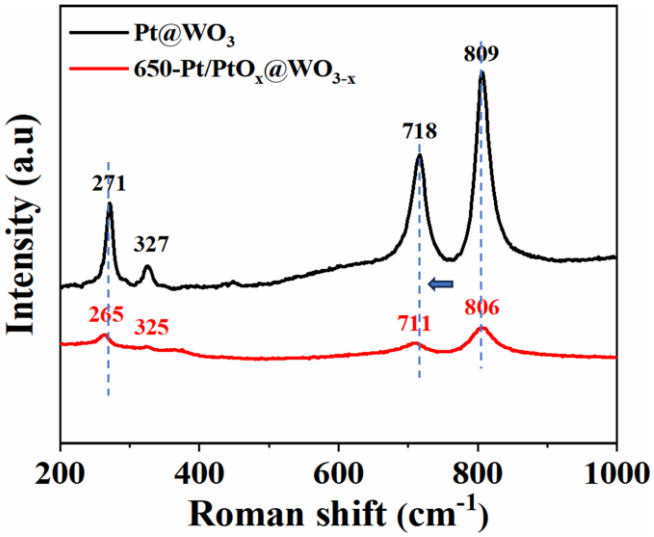

Figure S6. Raman spectra of $Pt@WO_3$ and $650\text{-}Pt/PtO_x@WO_{3-x}$.

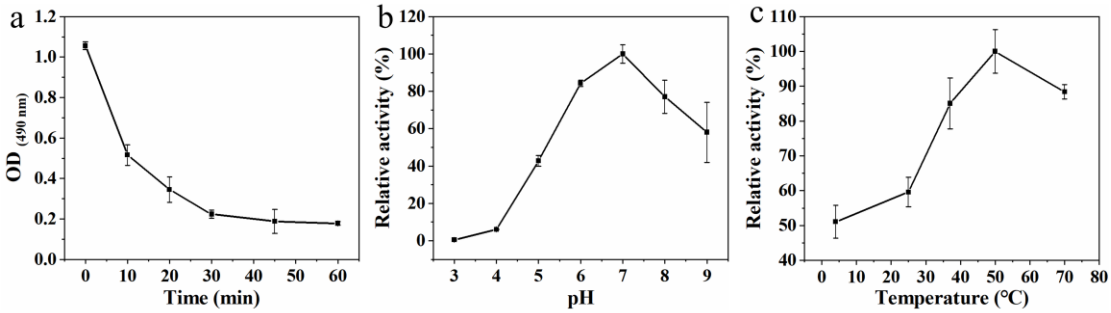

Figure S7. Catalytic activity of $650\text{-}Pt/PtO_x@WO_{3-x}$ for NADH at (a) time (b) pH values of 3.0-10.0 and (c) temperatures of 4-70 °C.

The kinetics of NADH oxidation were analyzed by measuring the time-dependent decrease in NADH using the MTS colorimetric assay at various initial concentrations.

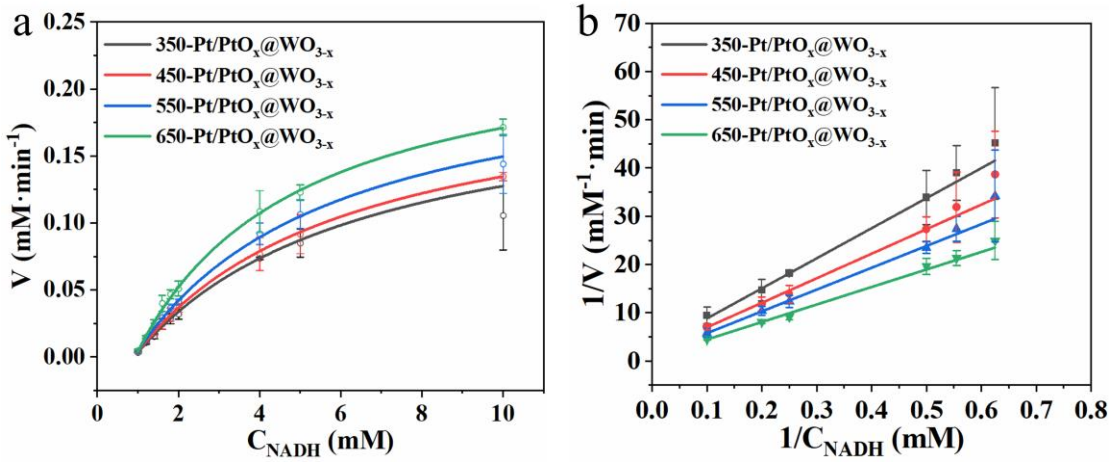

Figure S8. Steady-state kinetic and Lineweaver-Burk plots of $Pt/PtO_x@WO_{3-x}$.

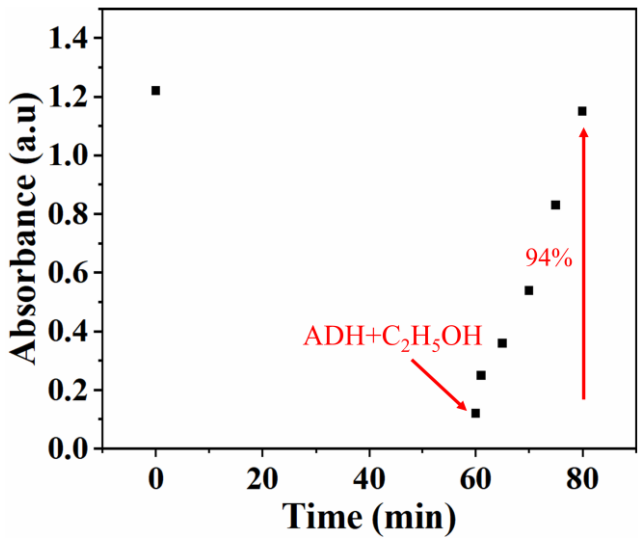

Figure S9. Time-dependent absorption intensity of NADH.

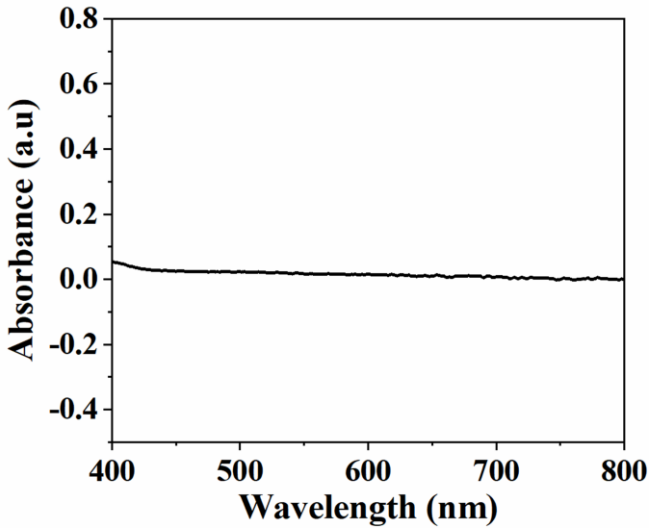

Figure S10. The UV-Vis absorption spectra of the solutions with incubating 650-Pt/PtO_x@WO_{3-x} and NADH for 60 minutes after adding HRP and TMB.

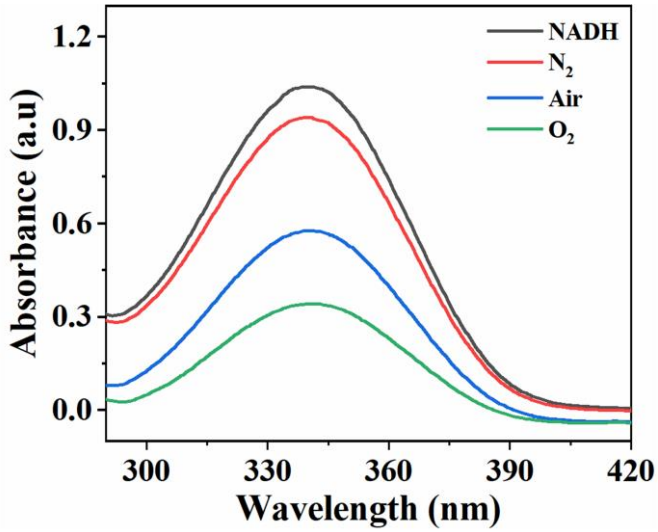

Figure S11. Effect of N_2, O_2, and Air on NADH oxidation.

Tryptophan (Trp), isopropanol (IPA), and trichloromethane (TCM) were used to identify the generation of singlet oxygen ($^1O_2$), hydroxyl radicals (•OH), and superoxide anions ($•O_2^-$), respectively.

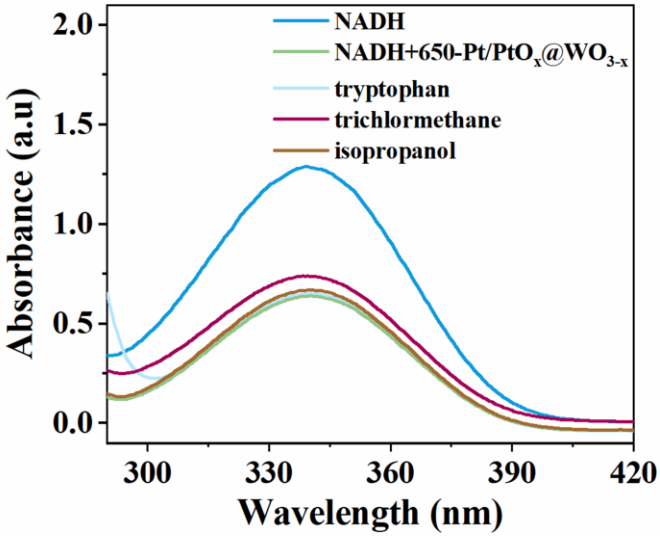

Figure S12. The effect of radical scavengers on the oxidation of NADH.

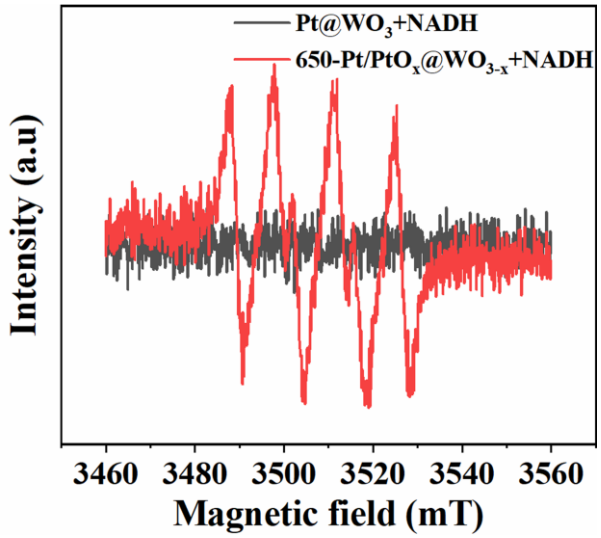

Figure S13. EPR spectra of the $\bullet O_2^-$.

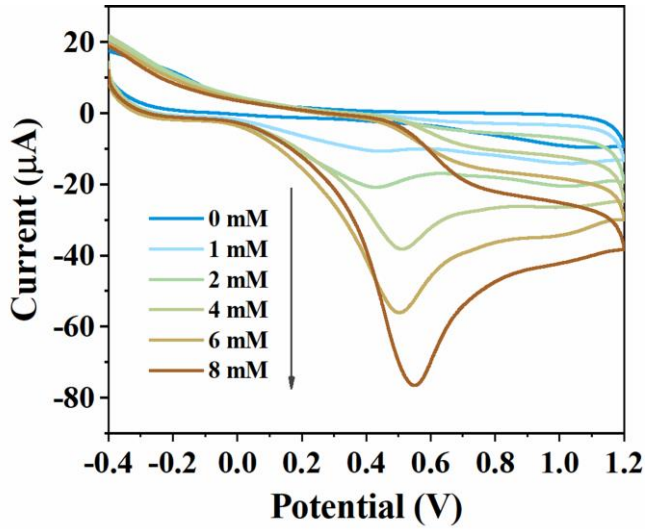

Figure S14. CV plots of 650-Pt/PtO_x@WO_{3-x}/GCE with different concentrations of NADH.

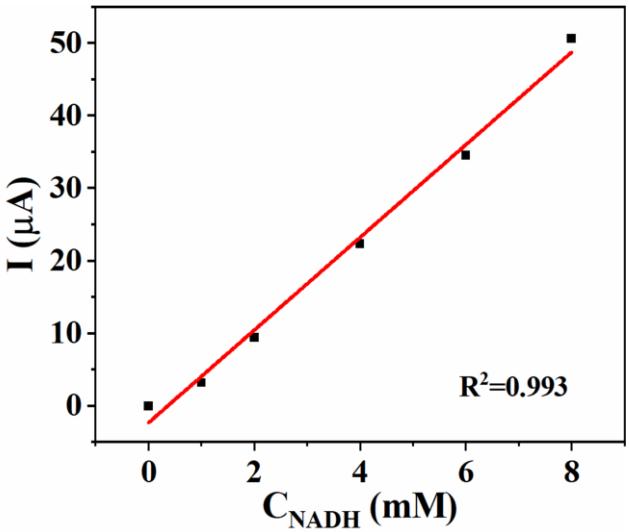

Figure S15. Variation of current with NADH concentration.

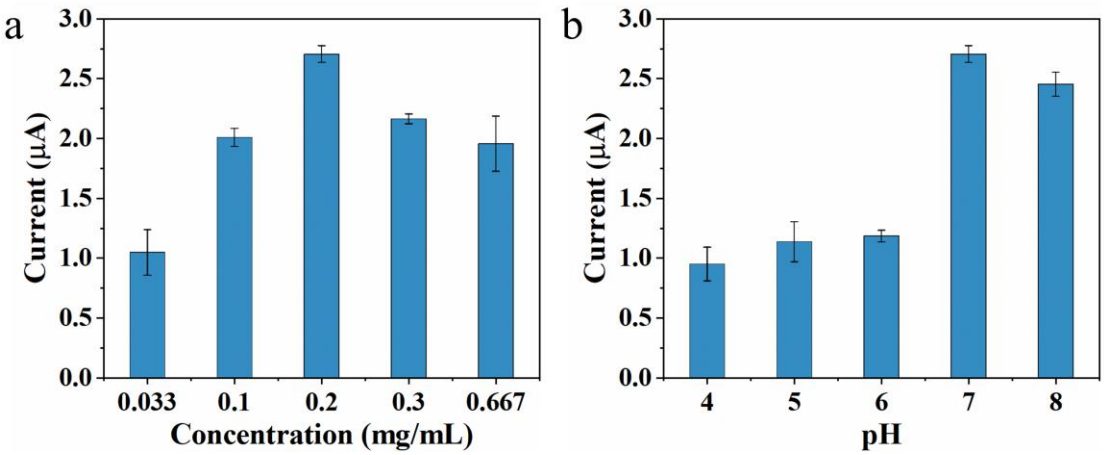

Figure S16. Effects of (a) enzyme concentrations and (b) pH towards detection of HB.

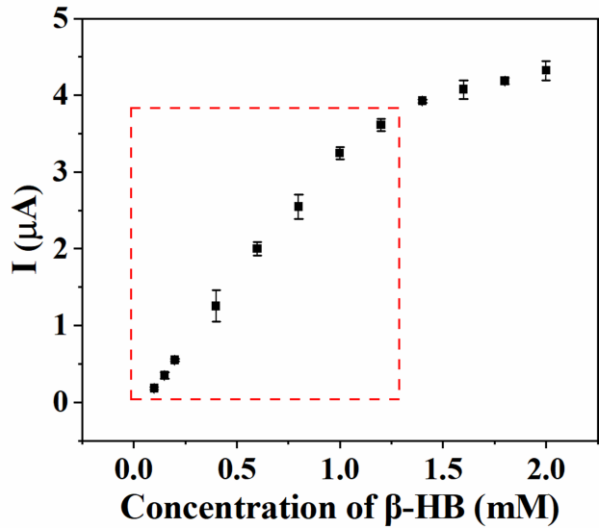

Figure S17. The current responses of the HBD-NAD^+/650-Pt/PtO_x@WO_{3-x}/GCE towards different concentrations of HB.

To further assess selectivity of the sensor, common interfering substances in human serum such as ascorbic acid, glucose, lactic acid, and uric acid were tested alongside 0.5 mM HB.

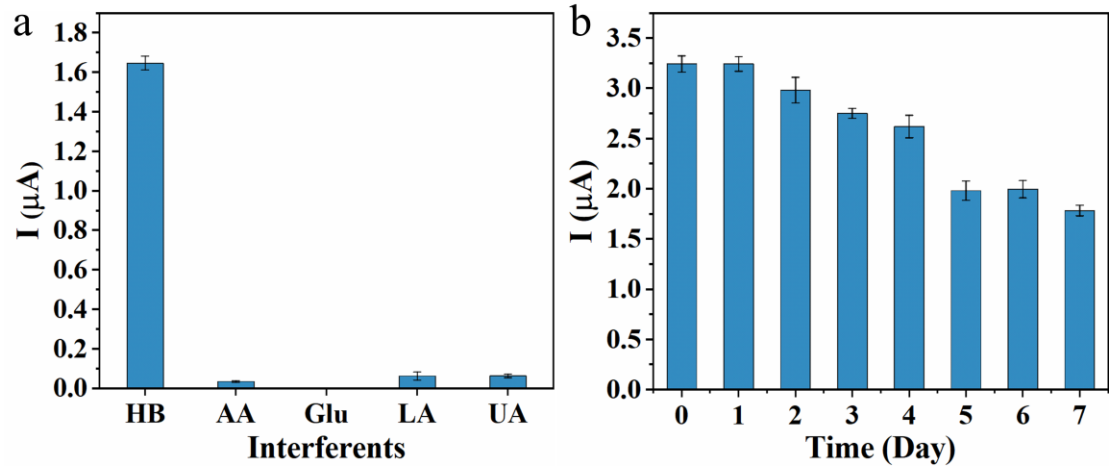

Figure S18. Selectivity(a) and stability(b) of the HBD-NAD^+/650-Pt/PtO_x@WO_{3-x}/GCE.

Table S1. Calculation of the percentage of Pt^{4+}, Pt^{2+} and Pt^0 from XPS spectra.

	Pt^{4+}	Pt^{2+}	Pt^0
Pt@WO_3	-	-	100%
350-Pt/PtO_x@WO_{3-x}	-	48.09%	51.91%
450-Pt/PtO_x@WO_{3-x}	-	64.80%	35.20%
550-Pt/PtO_x@WO_{3-x}	44.06%	31.75%	24.17%
650-Pt/PtO_x@WO_{3-x}	55.16%	32.42%	12.43%

Table S2. Calculation of the percentage of W^{5+}, W^{6+} from XPS spectra.

	W^{5+}	W^{6+}
Pt@WO_3	6.98%	94.06%
350-Pt/PtO_x@WO_{3-x}	8.30%	92.70%
450-Pt/PtO_x@WO_{3-x}	10.52%	89.48%
550-Pt/PtO_x@WO_{3-x}	13.76%	86.33%
650-Pt/PtO_x@WO_{3-x}	21.25%	78.75%

Table S3. Calculation of the percentage of lattice oxygen (O_L) and oxygen vacancies (O_V) from XPS spectra.

	O_L	O_V
$Pt@WO_3$	90.18%	9.82%
$350\text{-}Pt/PtO_x@WO_{3-x}$	73.12%	26.88%
$450\text{-}Pt/PtO_x@WO_{3-x}$	68.18%	31.82%
$550\text{-}Pt/PtO_x@WO_{3-x}$	66.01%	33.99%
$650\text{-}Pt/PtO_x@WO_{3-x}$	37.25%	62.75%

Table S4. Kinetic parameter of $Pt/PtO_x@WO_{3-x}$.

$Pt/PtO_x@WO_{3-x}$	K_m (mM)	V_{max} ($mM \cdot min^{-1}$)	K_{cat} (min^{-1})	K_{cat}/K_m ($min^{-1} \cdot mM^{-1}$)
350	4.6584	0.2057	200.61	43.06
450	4.3521	0.2123	207.05	47.57
550	3.9782	0.2299	224.21	56.36
650	3.0294	0.2457	239.62	79.10

Table S5. Accuracy of the constructed biosensors for real samples (n=3).

Add (mM)	Found (mM)	Recovery (%)	RSD (%)
0.3	0.299	99.6	2.8
0.6	0.606	101.1	1.7
1.0	1.008	100.8	1.6

Table S6. Some electrochemical enzyme biosensors for the determination of HB.

Electrode	Linear Range (mM)	LOD (mM)	Ref.
$HBD/NAD^+/SWCNTs/SPCE$	0.01-0.1	0.009	[7]
Bi-Enzyme-Based Clark Electrode	0.008-0.8	0.0039	[8]
$PD/NAD^+/HBD/EPAD$	0.1-6	0.3	[9]
HBD/THI/rGO/SPCE	0.003-0.4	0.001	[10]
$Mxene\text{-}HBD\text{-}NAD^+\text{-}GA\text{-}BSA$	0.36-17.9	0.045	[11]
$HBD\text{-}NAD^+/650\text{-}Pt/PtO_x@WO_{3-x}/GCE$	0.1-1.2	0.025	This work

References

1. L. Xiao, G. Li, Z. Yang, K. Chen, R. Zhou, H. Liao, Q. Xu and J. Xu, *Advanced Functional Materials*, 2021, **31**, 2100982.

2. G. Kresse and J. Furthmüller, *Computational Materials Science*, 1996, **6**, 15-50.

3. J. P. Perdew, K. Burke and M. Ernzerhof, *Physical Review Letters*, 1996, **77**, 3865-3868.

4. S. Grimme, S. Ehrlich and L. Goerigk, *Journal of Computational Chemistry*, 2011, **32**, 1456-1465.

5. T. A. A. Batchelor, J. K. Pedersen, S. H. Winther, I. E. Castelli, K. W. Jacobsen and J. Rossmeisl, *Joule*, 2019, **3**, 834-845.

6. K. Momma and F. Izumi, *Journal of Applied Crystallography*, 2011, **44**, 1272-1276.

7. F. Khorsand, M. Darziani Azizi, A. Naeemy, B. Larijani and K. Omidfar, *Molecular Biology Reports*, 2013, **40**, 2327-2334.

8. R. C. H. Kwan, P. Y. T. Hon, W. C. Mak, L. Y. Law, J. Hu and R. Renneberg, *Biosensors and Bioelectronics*, 2006, **21**, 1101-1106.

9. C.-C. Wang, J. W. Hennek, A. Ainla, A. A. Kumar, W.-J. Lan, J. Im, B. S. Smith, M. Zhao and G. M. Whitesides, *Analytical Chemistry*, 2016, **88**, 6326-6333.

10. G. Martínez-García, E. Pérez-Julián, L. Agüí, N. Cabré, J. Joven, P. Yáñez-Sedeño and J. M. Pingarrón, *Journal*, 2017, **7**.

11. A. Koyappayil, S. G. Chavan, M. Mohammadniaei, A. Go, S. Y. Hwang and M.-H. Lee, *Microchimica Acta*, 2020, **187**, 277.